Japanese Journal of Applied Physics

The Japan Society of Applied Physics

REGULAR PAPER • OPEN ACCESS

Initial stage of InSb heteroepitaxial growth on GaAs (111)A: effect of thin InAs interlayers

To cite this article: Akihiro Ohtake and Takaaki Mano 2024 *Jpn. J. Appl. Phys.* **63** 03SP10

OPEN ACCESS

Japanese Journal of Applied Physics **63**, 03SP10 (2024) **REGULAR PAPER**

https://doi.org/**10.35848/1347-4065/ad2032**

Initial stage of InSb heteroepitaxial growth on GaAs (111)A: effect of thin InAs interlayers

Akihiro Ohtake* and Takaaki Mano*

National Institute for Materials Science, 1-1 Namiki, Tsukuba, Ibaraki 305-0044, Japan

*E-mail: OHTAKE.Akihiro@nims.go.jp; MANO.Takaaki@nims.go.jp

Received December 11, 2023; revised January 15, 2024; accepted January 18, 2024; published online February 8, 2024

MBE of InSb on the (111)A-oriented GaAs substrates has been studied using electron diffraction, X-ray diffraction, and scanning probe microscopy. The direct heteroepitaxial growth of InSb on GaAs(111)A results in a cracked morphology with flat terraces and deep gaps, which could be attributed to the extremely large lattice mismatch between InSb and GaAs (14.6%). When thin (5–30 monolayer thickness) InAs films are used as interlayers, more continuous and flat InSb films are obtained. The proposed growth technique using (111)A-oriented GaAs substrates and thin InAs interlayers are effective in improving the surface morphology and the structural quality of InSb films in highly lattice-mismatched systems.

1. Introduction

III–V semiconductors with narrow band gaps, such as InAs, GaSb, and InSb, are essential materials for various device application due to their high mobility characteristic and optical properties at IR region. As the examples, Hall sensors, IR-photosensors, and IR LEDs have been developed and commercialized.[1–7] The wafers of InAs, GaSb, and InSb are normally very expensive and large-size wafers are not available. In addition, the narrow-gap semiconductor substrates can be a source of parallel conduction when used as substrates for lateral conductive devices.[8] Therefore, heteroepitaxial growth of these narrow gap III–V semiconductors on versatile lattice-mismatched substrates (Si, GaAs, or InP) with wider band gap has been important research topic for more than three decades.[8–12] InSb has a highest electron mobility (~78 000 $cm^2\ V^{-1}\ s^{-1}$) and a very narrow band gap (0.17 eV at 300 K) among the III–V semiconductors, making itself promising for applications in magnetic field sensing and mid-IR light detection with high sensitivity. However, a large lattice constant of InSb (0.6479 nm) causes difficulty in growing high quality layers on GaAs substrates whose lattice constant is 14.6% smaller than that of InSb. On the standard GaAs (100) substrates, several techniques have been developed to improve the quality, such as anion exchange (Sb soaking)[12–14] and/or two-step growth (temperature variation).[7,15–18] It has been reported that most of the dislocations induced by the lattice mismatch could be confined at the interface of InSb/GaAs by utilizing these growth technique,[16] and that high mobility characteristics have been realized in relatively thick InSb layers grown on GaAs(100).[8,15,18,19] However, three-dimensional islands are often formed at the initial stage of the InSb growth, which degrade the structural and electrical properties of thinner InSb films.[20,21] Since device structures with thin InSb layer are effective in reducing the cost, and are also preferred for specific applications using magnetoresistance,[8,20] the initial island growth should be suppressed.

Kanisawa et al. have proposed to use the (111)A-oriented GaAs substrate to obtain smooth surface from the beginning of the InSb growth.[21] Earlier studies have shown that in the lattice-mismatched system of InAs on GaAs(111)A, the formation of three-dimensional islands is effectively inhibited by introducing misfit-dislocation network at the interface.[22–25] The layer-by-layer growth continues throughout the growth, which is in stark contrast to that for the (100) orientation where Stranki-Krastanow growth occurs.[26–28] The layer-by-layer growth was also realized for InSb on GaAs(111)A by combining the two-step growth technique, and the 200 nm thick InSb layer exhibits mobility close to ~10 000 $cm^2\ V^{-1}\ s^{-1}$.[21] On the other hand, atomic force microscopy (AFM) observations showed that three-dimensional structures (density: ~$10^8\ cm^{-2}$) were actually formed on the 30 nm thick InSb layers.[21] This means that further studies are required for the growth of thin InSb layers on GaAs (111)A in order to improve the crystal quality.

In this study, we investigate the initial growth stage of InSb on GaAs(111)A in detail. We focus on the low-temperature growth of InSb which corresponds to the first step of the two-step growth. By studying strain relaxation processes and surface morphology of InSb, we found that the direct growth of InSb on GaAs(111)A causes a rough surface which consists of terraces and deep gaps. To suppress the gap formation, we propose the growth method using InAs interlayers, which has been developed for growing InGaAs on GaAs(111)A, GaSb on GaAs(111)A, and GaSb on Si(111).[29–31] By introducing thin InAs interlayers, flat surfaces of InSb(111)A could be formed even at the early stage of the growth.

2. Experimental methods

The growth experiments were carried out in a system of interconnecting ultrahigh vacuum (UHV) chambers for MBE and for on-line surface characterization by means of scanning tunneling microscopy (STM).[32] The InSb films were grown on the GaAs(111)A substrates with and without thin InAs layers. The samples were also grown on the InAs(111)A substrate for comparison. The clean surfaces of GaAs(111)A and InAs(111)A were prepared by growing undoped homoepitaxial layers at 450 °C on the thermally cleaned substrates.[33] The GaAs (InAs) layers were grown with an As_4/Ga (As_4/In) flux ratio of ~50. The cleaned GaAs and

InAs surfaces show a (2 × 2) reconstruction. Thin InAs layers on GaAs(111)A were also grown under otherwise identical conditions.

InSb films were grown at substrate temperatures of 300 °C and 320 °C. The beam-equivalent pressures (BEPs) of In and Sb were measured using a beam flux monitor at the sample position. The BEP of In was fixed at $\sim 9 \times 10^{-7}$ Pa. On the other hand, because of the lower sticking probability of Sb molecules at a higher temperature of 320 °C, the BEPs for Sb was controlled to $\sim 5 \times 10^{-6}$ Pa and $\sim 1.5 \times 10^{-5}$ Pa for the growth at 300 °C and 320 °C, respectively. Prior to the InSb growth at 320 °C, the initial substrate surface was exposed to the Sb molecular beam for 20 s. Under either growth condition, the growing surface shows an In-stabilized (2 × 2) reconstruction at the initial stage of the growth, and an Sb-stabilized $(2\sqrt{3} \times 2\sqrt{3})$R30° phase begins to coexist above ∼20 monolayer (ML)-thickness. The appearance of the $(2\sqrt{3} \times 2\sqrt{3})$R30° reconstruction indicates that the InSb film grows with a (111)A orientation.[34] The samples showed (2 × 2) surfaces after interrupting the In and Sb molecular beams at growth temperatures, and were then transferred via UHV transfer modules to another chamber for the on-line characterizations by STM. The growth rate of InSb was approximately 0.03 ML s^{-1}, which was calibrated by reflection high-energy electron diffraction (RHEED) intensity oscillation measurements for the (001)-oriented InAs growth. Here, 1 ML of InSb is defined as 5.5×10^{14} atoms cm^{-2}, which is the site-number density of unreconstructed InSb(111)A surface.

The growth processes were monitored by in situ RHEED with electron- beam energy of 15 keV. All the STM images were collected at RT in the constant current mode with a tunneling current of 0.1 nA and a sample voltage of −3 V. The samples were also characterized by AFM, and X-ray diffraction (XRD). High resolution XRD measurements were carried out using a monochromatic Cu Kα1 radiation. A channel-cut analyzer crystal was used for X-ray rocking curve (XRC) measurements.

Results and discussion

Figure 1 shows RHEED patterns taken before and after the growth of InSb (50 ML thickness) on GaAs(111)A (a and b), 10 ML-InAs/GaAs(111)A (c and d), and InAs(111)A (e and f) substrates at 320 °C. Since sharp and intense streaks were observed, one may expect that high-quality InSb films with flat surfaces were grown on all substrates. However, the surface morphology critically depends on the type of substrate, as we will show later. From the spacing of the streaks, the in-plane lattice constant of the InSb(111)A film is roughly estimated to be 0.46 nm, which is quite close to the bulk value (0.458 nm).

Figure 2(a) shows the in-plane lattice constant (d_{110}) of the InSb film grown on the GaAs(111)A substrate at 300 °C and 320 °C plotted as a function of the InSb film thickness. The d_{110} values were measured from the distance between the 1 1 and $\bar{1}1$ reflections in the RHEED patterns taken along the $[11\bar{2}]$ direction. The reflections from InSb film appeared at 1.5 ML thickness, in addition to those from the GaAs substrate. The d_{110} values of the InSb film are quite close to the value of bulk InSb, and remains almost unchanged throughout the growth. This indicates that the InSb film was nucleated with its inherent lattice constant, and that pseudomorhic InSb layers are not formed. Thus, it is likely that the lattice mismatch of InSb/GaAs(111)A (14.6%) is too large to be accommodated by elastic deformation of thin InSb films, similarly to the case for InAs/Si (11.5%).[24]

To reduce the lattice mismatch between InSb and GaAs, the growth experiments were carried out using thin InAs interlayers. Figures 2(b)–2(e) show the variation of d_{110} value for the InSb growths on 5 ML-, 10 ML-, 20 ML-, and 30 ML-thick InAs layers on GaAs(111)A. As already reported,[23,24] the in-plane lattice constants of InAs on GaAs(111)A increases with InAs film thickness: the d_{110} values of the 5 ML-, 10 ML-, 20 ML-, and 30 ML-thick InAs films are roughly estimated to be 0.418, 0.421, 0.422, and 0.423 nm, respectively.

As can be seen in Figs. 2(b)–2(e), the insertion of InAs layer drastically changes the strain relaxation process of InSb: the d_{110} value begins to change at the very early stage of the growth (0.2–0.5 ML thickness), and gradually increase as the growth proceeds. In the InSb/InAs system with a smaller lattice mismatch of 7.0%, as shown in Fig. 2(f), the d_{110} value begins to change at ∼1 ML, and increases with InSb thickness: the observed variation in d_{110} is similar to that for InAs/GaAs(111)A (7.1%).[22,23] On the other hand, strain state is different between the two systems: the strain in the InAs film on GaAs(111)A has relaxed by only ∼80% after the 50 ML-growth, while the 50 ML-InSb film on InAs(111)A is mostly relaxed.

Here, it is interesting to note that the strain relaxation proceeds more rapidly for thinner InAs thickness. Thus, it is

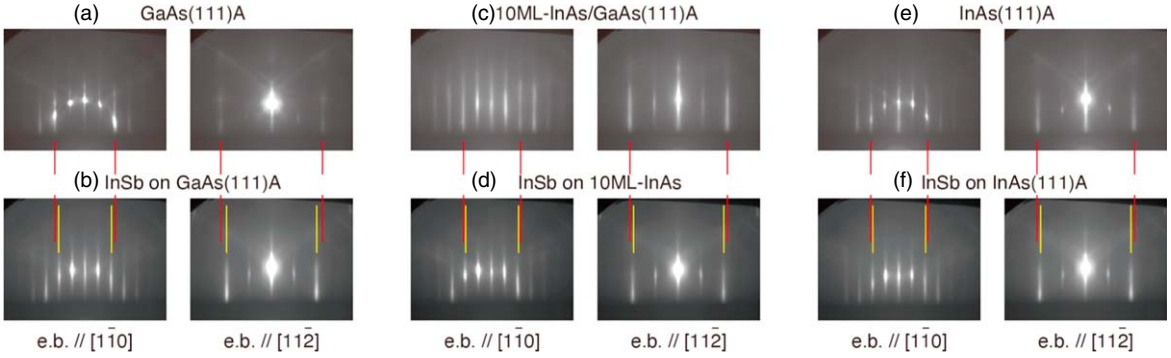

Fig. 1. RHEED patterns of before and after the growth of 50 ML-InSb films on GaAs(111)A (a) and (b), 10 ML-InAs/GaAs(111)A (c) and (d), and InAs (111)A (e) and (f) substrates. The growth temperature was 320 °C. The electron-incidence azimuths are $[1\bar{1}0]$ and $[11\bar{2}]$. Vertical lines indicate the position of the streaks.

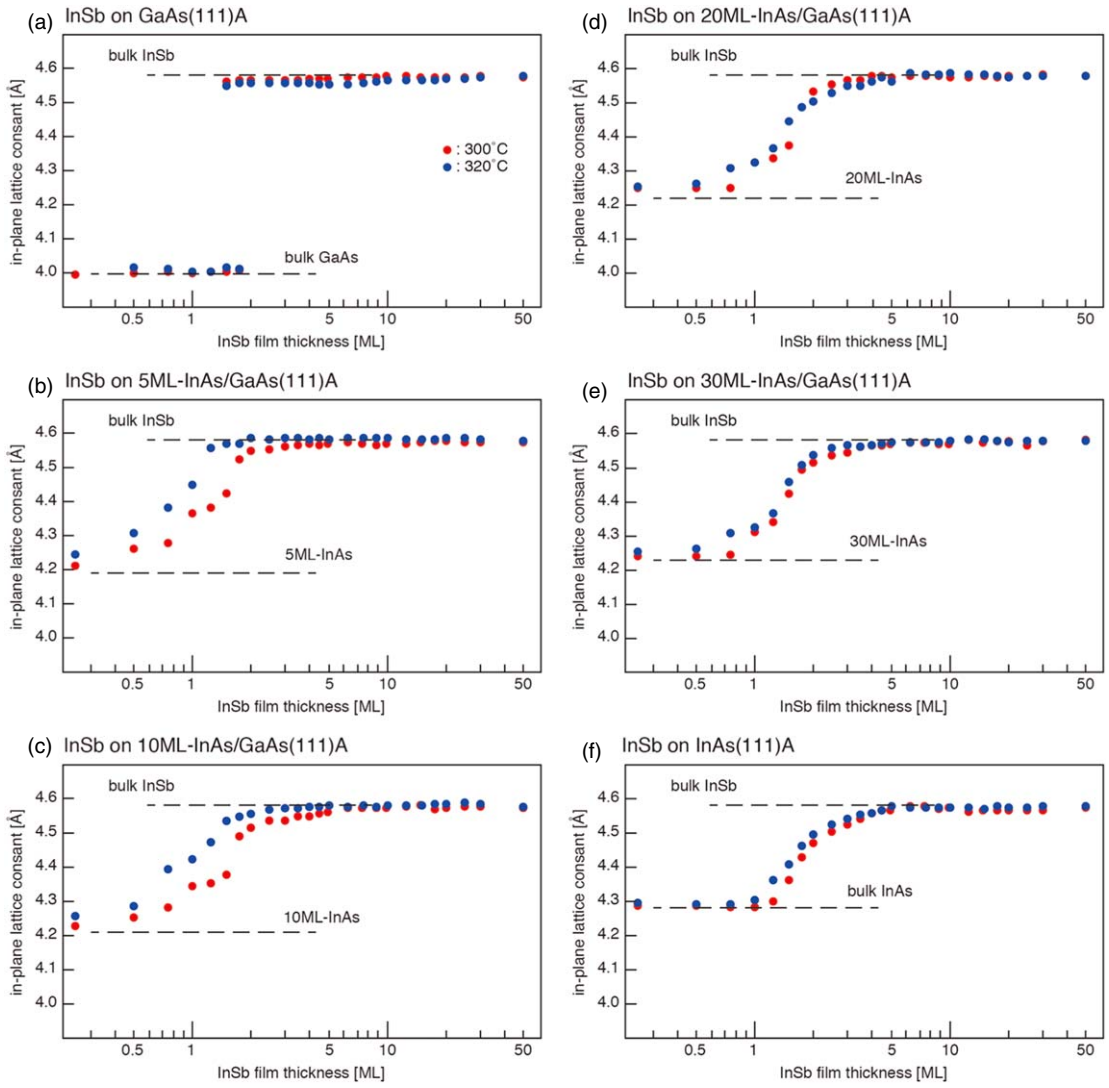

Fig. 2. Variation of the in-plane lattice constant (d_{110}) of InSb films grown on GaAs(111)A (a), InAs/GaAs(111)A (b)–(e), and InAs(111)A (f) substrates. The values were measured from the distance between the 1 1 and $\bar{1}1$ reflections in the RHEED patterns. Red and blue circles represent the results for the growth at 300 °C (BEP of Sb: $\sim 5 \times 10^{-6}$ Pa) and 320 °C (BEP of Sb: $\sim 1.5 \times 10^{-5}$ Pa), respectively. The horizontal dashed lines indicate the d_{110} values of the substrates and bulk InSb.

possible that thin InAs interlayer is elastically deformed to accumulate compressive strain in InSb layers, as already found in InGaAs on InAs/GaAs(111)A.[30] Another interesting finding is that the strain relaxation is delayed at a lower temperature of 300 °C. Since, as mentioned earlier, the InSb growth at 320 °C was carried out under more Sb-rich conditions: the higher Sb flux of 1.5×10^{-7} Pa was used and the initial surface was exposed to the Sb flux prior to the growth. Thus, it is suggested that Sb atoms are more preferentially incorporated in InAs layers at the initial stage of the InSb growth at 320 °C to form an InAsSb-like phase, which promotes the strain relaxation of InSb.

Figures 3(a) and 3(b) show STM and AFM images, respectively, observed for the 50 ML thick InSb film directly grown on GaAs(111)A at 320 °C. While the surface consists of terraces with a typical width of several tens of nm, deep gaps are frequently observed. The depth of the gap is roughly estimated to be ∼20 nm, being consistent with the thickness of the 50 ML-InSb film. The rms roughness (R_q) values are 2.56 and 3.36 nm for STM (a) and AFM (b) images, respectively. The existence of the gap indicates that the direct InSb growth on GaAs(111)A proceeds with the formation of large two-dimensional islands, but not with a layer-by-layer mode.

The insertion of thin InAs layer is effective to improve the surface morphology of InSb films. The STM and AFM images of InSb films grown with InAs interlayers (5 ML and 30 ML) are shown in Figs. 3(c)–3(f). The surfaces show atomically flat terraces separated by steps with the height of ∼0.37 nm, which corresponds to the ML height of InSb(111): while shallow holes are formed on terraces, no deep gap was observed. The R_q values are significantly deceased, and are smaller than 0.5 nm in the whole range of InAs thickness between 5 and 30 ML. As shown in Figs. 3(g) and 3(h), the InSb film grown on the InAs substrate also shows a flat surface with small R_q values of 0.20 nm (g) and 0.39 nm (h). These results indicate that the reduction of the lattice mismatch by inserting thin InAs layers is crucial in obtaining better surface morphology of epitaxial InSb films. Here we note that the difference in surface morphologies could not be assessed by RHEED observations: as shown in Figs 1(b), 1(d), and 1(f), the InSb films grown on GaAs(111)A (a), 10

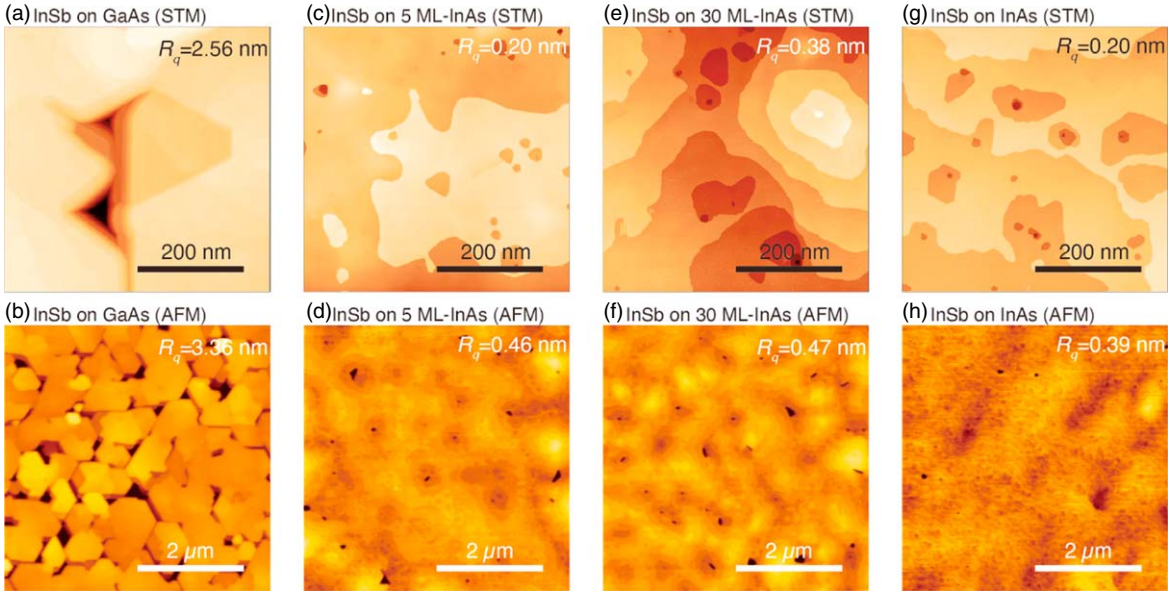

Fig. 3. Typical filled-state STM images and AFM images of 50 ML-InSb films grown on GaAs(111)A (a) and (b), InAs/GaAs(111)A (c)–(f), and InAs(111)A (g) and (h) substrates. The growth temperature was 320 °C. Image dimensions of STM and AFM images are 500 nm × 500 nm and 5 μm × 5 μm, respectively. Black to white represents the height difference of 23 nm (a), 25 nm (b), 2 nm (c), 5 nm, (d), 3 nm (e), 5 nm (f), 3 nm (g), and 3 nm (h).

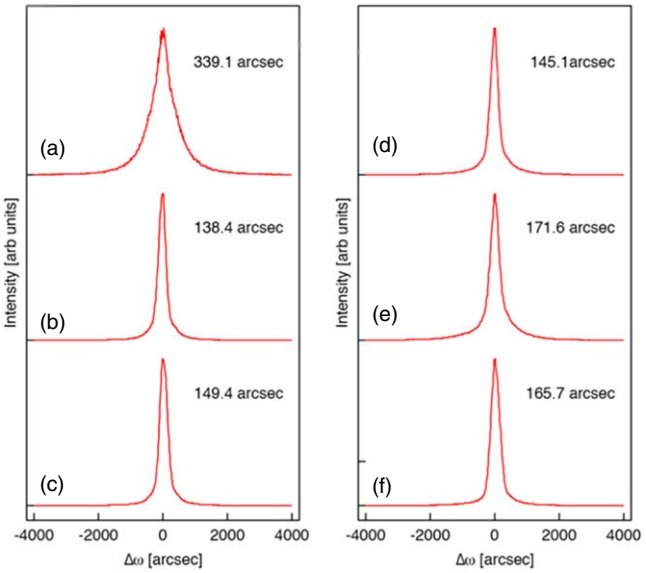

Fig. 4. Symmetric 111 XRCs of 100 nm InSb films grown on GaAs(111)A (a), 5 ML-InAs/GaAs(111)A (b), 10 ML-InAs/GaAs(111)A (c), 20 ML-InAs/GaAs(111)A (d), 30 ML-InAs/GaAs(111)A (e), and InAs(111)A (f) substrates. The growth temperature was 300 °C.

ML-InAs/GaAs(111)A (b), and InAs(111)A (c) substrates show quite similar RHEED patterns.

To investigate the crystalline quality of the InSb film, we carried out XRD measurements for the 100 nm thick InSb films prepared under identical growth conditions at 300 °C. Figures 4(a)–4(f) compares XRCs of the symmetric 111 reflection measured from 100 nm InSb films. The FWHM value of the InSb film directly grown on GaAs(111)A is 339 arcsec. For the InSb films grown using InAs interlayers, the FWHM values are less than 200 arcsec, showing a better crystallinity, indicating that the thin InAs layer is also effective in improving the structural properties of InSb. We have reported that the residual strain in epitaxial films gives rise to the peak broadening in XRC profiles.[24,29] However, since the 100 nm-InSb film on GaAs(111)A is almost relaxed (99.7%), the observed peak broadening could not be explained on the basis of residual strain. On the other hand, the broader XRC profile is compatible with the STM and AFM results: as can be seen in Figs. 3(a) and 3(b), the InSb film directly grown on GaAs substrate consists of two-dimensional islands separated by gaps, while those grown on InAs are more continuous. Since the XRC width generally increases as the domain size decreases, the improvement in the film morphology is likely to be responsible for the narrower FWHM width in Figs. 4(b)–4(f).

4. Conclusions

We have studied the strain relaxation processes InSb on GaAs(111)A with a large lattice mismatch of 14.6%. The fully-relaxed InSb film starts to grow directly on the GaAs (111)A substrate, resulting in the rather defective film quality. The insertion of the thin InAs layers (5–30 ML in thickness) significantly changes the strain relaxation processes and improve the surface morphology and the structural quality of the InSb films. The heteroepitaxial growth technique using thin InAs layers is promising for the realization of InSb-based devices on the low-cost GaAs wafers.

Acknowledgments

The authors are grateful to Drs. T. Kawazu, H. T. Miyazaki, and Y. Sakuma for their fruitful discussion.

ORCID iDs

Akihiro Ohtake https://orcid.org/0000-0002-3519-4613
Takaaki Mano https://orcid.org/0000-0002-6955-260X

1) G. Singh, E. Michel, C. Jelen, S. Slivken, J. Xu, P. Bove, I. Ferguson, and M. Razeghi, J. Vac. Sci. Technol. B **13**, 782 (1995).
2) I. Shibasaki, J. Cryst. Growth **175-176**, 13 (1997).
3) A. Okamoto, A. Ashihara, T. Akaogi, and I. Shibasaki, J. Cryst. Growth **227-228**, 619 (2001).
4) Rogalski, Opto-Electron. Rev. **20**, 279 (2012).
5) A. Krier, H. H. Gao, V. V. Sherstnev, and Y. Yakovlev, J. Phys. D: Appl. Phys. **32**, 3117 (1999).

6) H. Fujita, K. Ueno, O. Morohara, E. Camargo, H. Geka, Y. Shibata, and N. Kuze, Phys. Status Solidi A **215**, 1700449 (2018).
7) H. Lin, Z. Zhou, H. Xie, Y. Sun, X. Chen, J. Hao, S. Hu, and N. Dai, Phys. Status Solidi A **218**, 2100281 (2021).
8) T. Zhang, S. K. Clowes, M. Debnath, A. Bennett, C. Roberts, J. J. Harris, R. A. Stradling, L. F. Cohen, T. Lyford, and P. F. Fewster, Appl. Phys. Lett. **84**, 4463 (2004).
9) H. Yamaguchi, M. R. Fahy, and B. A. Joyce, Appl. Phys. Lett. **69**, 776 (1996).
10) K. Murata, N. B. Ahmad, Y. Tamura, M. Mori, C. Tatsuyama, and T. Tambos, J. Cryst. Growth **301–302**, 203 (2007).
11) A. Ohtake and K. Mitsuishi, J. Vac. Sci. Technol. B **29**, 031804 (2011).
12) M. D. Nordstrom, T. A. Garrett, P. Reddy, J. McElearney, J. R. Rushing, K. D. Vallejo, K. Mukherjee, K. A. Grossklaus, T. E. Vandervelde, and P. J. Simmonds, Cryst. Growth Des. **23**, 8670 (2023).
13) B. W. Jia, K. H. Tan, W. K. Loke, S. Wicaksono, and S. F. Yoon, J. Appl. Phys. **120**, 035301 (2016).
14) S. Huang, G. Balakrishnan, and D. L. Huffaker, J. Appl. Phys. **105**, 103104 (2009).
15) M. C. Debnath, T. Zhang, C. Roberts, L. F. Cohen, and R. A. Stradling, J. Cryst. Growth **267**, 17 (2004).
16) T. W. Kim, H. C. Bae, and H. L. Park, Appl. Phys. Lett. **74**, 380 (1999).
17) J. L. Davis and P. E. Thompson, Appl. Phys. Lett. **54**, 2235 (1989).
18) E. Michel, G. Singh, S. Slivken, C. Besikci, P. Bove, I. Ferguson, and M. Razeghi, Appl. Phys. Lett. **65**, 3338 (1994).
19) S. Fujikawa, T. Taketsuru, D. Tsuji, T. Maeda, and H. I. Fujishiro, J. Cryst. Growth **425**, 64 (2015).
20) S. A. Solin, T. Thio, D. R. Hines, and J. J. Heremans, Science **289**, 1530 (2000).
21) K. Kanisawa, H. Yamaguchi, and Y. Hirayama, Appl. Phys. Lett. **76**, 589 (2000).
22) H. Yamaguchi, J. G. Belk, X. M. Zhang, J. L. Sudijono, M. R. Fahy, T. S. Jones, D. W. Pashley, and B. A. Joyce, Phys. Rev. B **55**, 1337 (1997).
23) A. Ohtake, M. Ozeki, and J. Nakamura, Phys. Rev. Lett. **84**, 4665 (2000).
24) A. Ohtake, T. Mano, and Y. Sakuma, Sci. Rep. **10**, 4606 (2020).
25) T. Mano, A. Ohtake, T. Kawazu, H. T. Miyazaki, and Y. Sakuma, ACS Appl. Mater. Interfaces **15**, 29636 (2023).
26) L. Goldstein, F. Glas, J. Y. Marzin, M. N. Charasse, and G. Le Roux, Appl. Phys. Lett. **47**, 1099 (1985).
27) D. Leonard, M. Krishnamurthy, C. M. Reaves, S. P. Denbaars, and P. M. Petroff, Appl. Phys. Lett. **63**, 3203 (1993).
28) Y. Nabetani, T. Ishikawa, S. Noda, and A. Sasaki, J. Appl. Phys. **76**, 347 (1994).
29) A. Ohtake, T. Mano, K. Mitsuishi, and Y. Sakuma, ACS Omega **3**, 15592 (2018).
30) T. Mano, K. Mitsuishi, N. Ha, A. Ohtake, A. Castellano, S. Sanguinetti, T. Noda, Y. Sakuma, T. Kuroda, and K. Sakoda, Cryst. Growth Des. **16**, 5412 (2016).
31) A. Ohtake, T. Mano, N. Miyata, T. Mori, and T. Yasuda, Appl. Phys. Lett. **104**, 032101 (2014).
32) A. Ohtake, Surf. Sci. Rep. **63**, 295 (2008).
33) A. Ohtake, N. Ha, and T. Mano, Cryst. Growth Des. **15**, 485 (2015).
34) A. J. Noreika, M. H. Francombe, and C. E. C. Wood, J. Appl. Phys. **52**, 7416 (1981).